Supplementary Information to:

Uncovered bathymetry under Antarctica's fourth largest ice shelf reveals potential for seasonal warm water inflow

This attachment consists of 10 Supplementary Figures in total. These are presented in the following order, according to their appearance in the main text:

Supplementary Figure 1. Detailed bathymetric model of Riiser-Larsen and Quar ice shelves.

Supplementary Figure 2. Water column thickness beneath Riiser-Larsen and Quar ice shelves.

Supplementary Figure 3. Ice base across Riiser-Larsen Ice Shelf from newly acquired ice penetrating radar data with focus on additional pinning point.

Supplementary Figure 4. Difference of the new modelled bathymetry to topographic compilation IBCSO V2.

Supplementary Figure 5: Overview of oceanographic data.

Supplementary Figure 6. Ice base across Riiser-Larsen Ice Shelf from newly acquired ice penetrating radar data with focus on subglacial channels.

Supplementary Figure 7. Ice base across Riiser-Larsen Ice Shelf from newly acquired ice penetrating radar data with focus on basal melt structures around the central pinning point.

Supplementary Figure 8. Ice base across Riiser-Larsen Ice Shelf from newly acquired ice penetrating radar data with focus on marine ice accretion.

Supplementary Figure 9. Bedrock density model used for inversion.

Supplementary Figure 10. Gravity residuals after modelling the Riiser-Larsen Ice Shelf cavity.

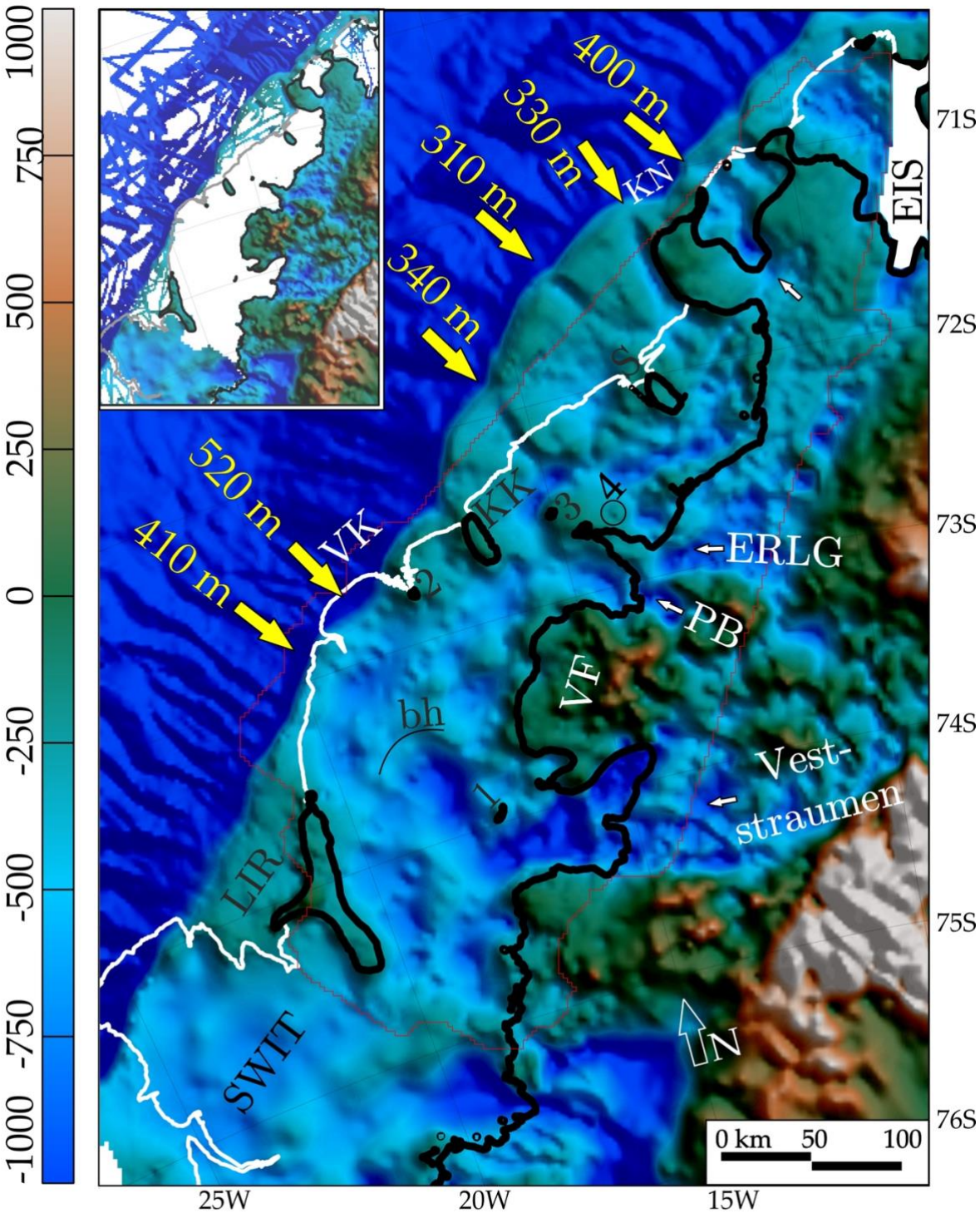

Supplementary Figure 1. Detailed bathymetric model of Riiser-Larsen and Quar ice shelves. White arrows show glaciers (PB, Plogbreen; ERLG, eastern Riiser-Larsen Glacier), topographic features are labelled (KK, Kvitkuven; KNor, Kapp Norvegia; LIR, Lyddan Ice Rise; 1 through 4, numbered pinning points; S, Skjoldet ice rise; VF, Vestfjella mountain site; VK, Vestkapp), as well as neighbouring ice shelves (EIS, Ekström Ice Shelf; SWIT, Stancomb-Wills ice Tongue). Red outline gives gridded airborne gravity data extent from Fig. 2a. Calving fronts and grounded areas are extracted from MEaSUREs data collection[1] and additional databanks[2].

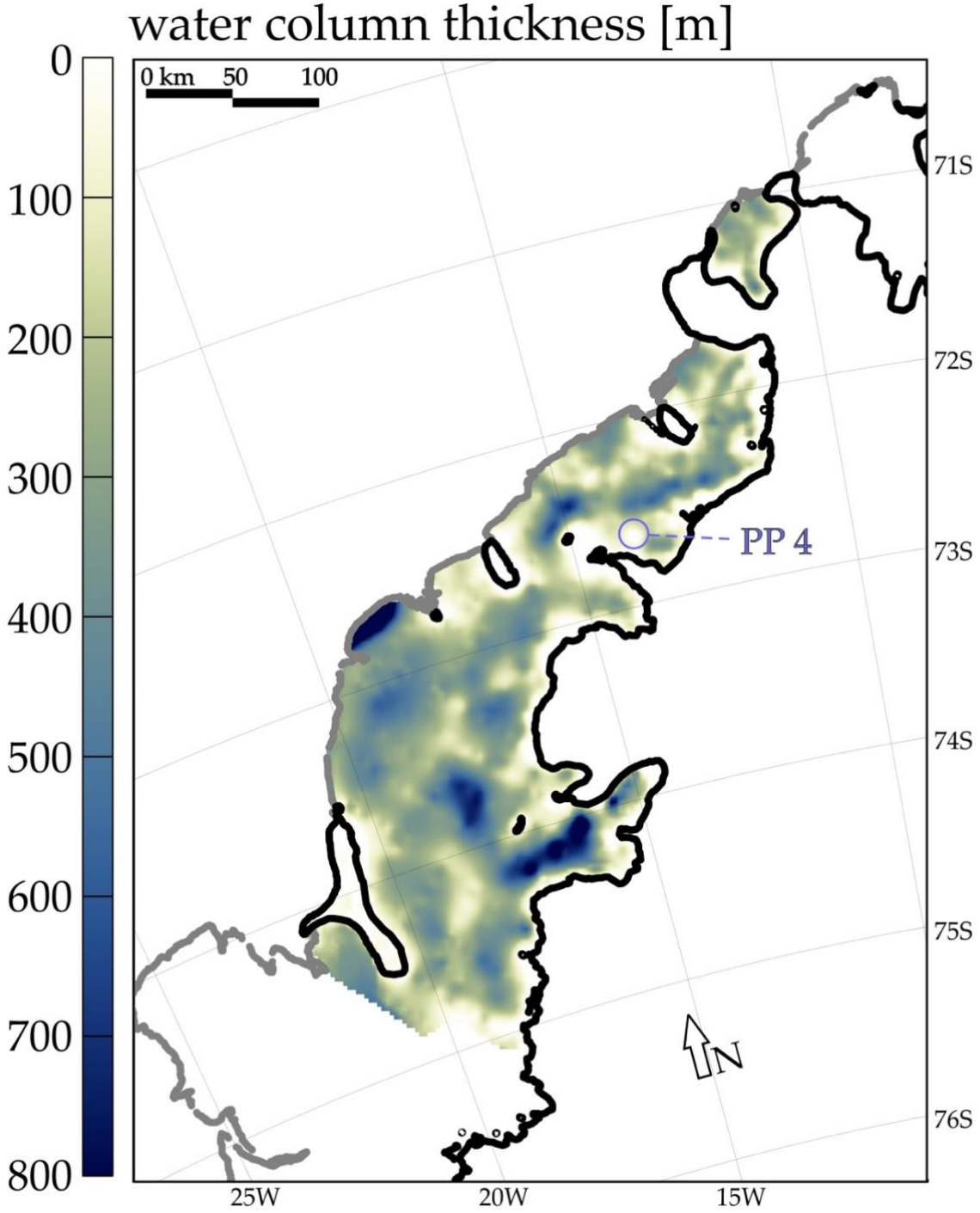

Supplementary Figure 2. Water column thickness beneath Riiser-Larsen and Quar ice shelves. It is calculated from the newly developed bathymetric model and the ice base inferred from ice penetrating radar data in Supplementary Fig. 3. Calving fronts and grounded areas are extracted from MEaSUREs data collection[1] and additional databanks[2].

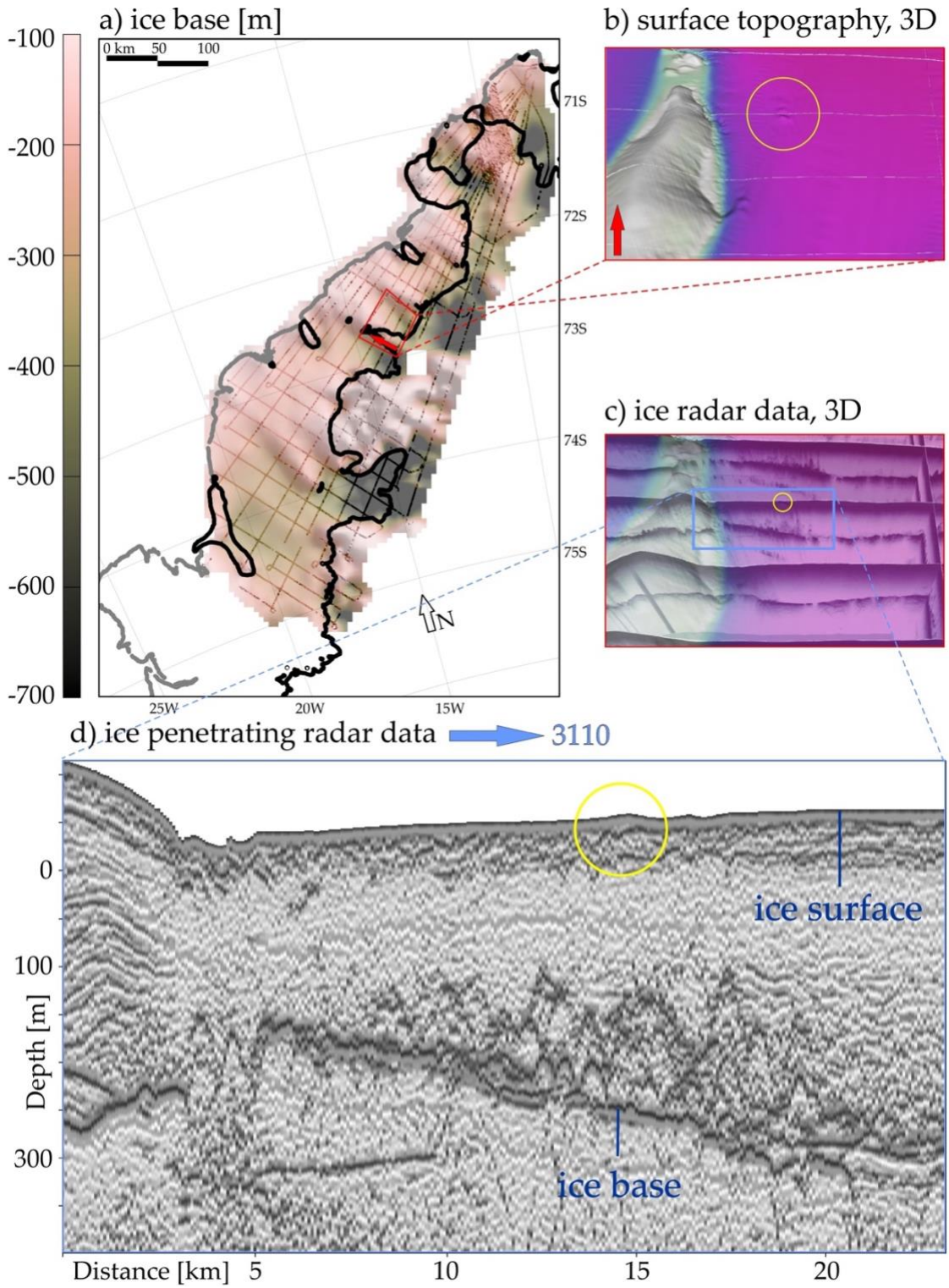

Supplementary Figure 3. Ice base across Riiser-Larsen Ice Shelf from newly acquired ice penetrating radar data with focus on additional pinning point. **(**a) shows ice base position across the survey area. A red bounding box here marks the proposed ice rise. A bump in surface height is observed in a three-dimensional view in (b) of digital elevation model REMA[3]. Its location is marked with a yellow circle here, as well as in (c) and (d). (c) shows available ice penetrating radar data of the same area in a three-dimensional view. Here, the along-flow progression of basal features is shown with distinct features initiating around the area of the proposed additional pinning point. The blue bounding box depicts the extent of the radargram (d) with a vertical exaggeration of ~25. It is an excerpt of line 20233110 and shows disruption of the ice base. While no disruption of the ice base is visible upstream of this profile, similar disruptions are visible downstream. Calving fronts and grounded areas in (a) are extracted from MEaSUREs data collection[1] and additional databanks[2].

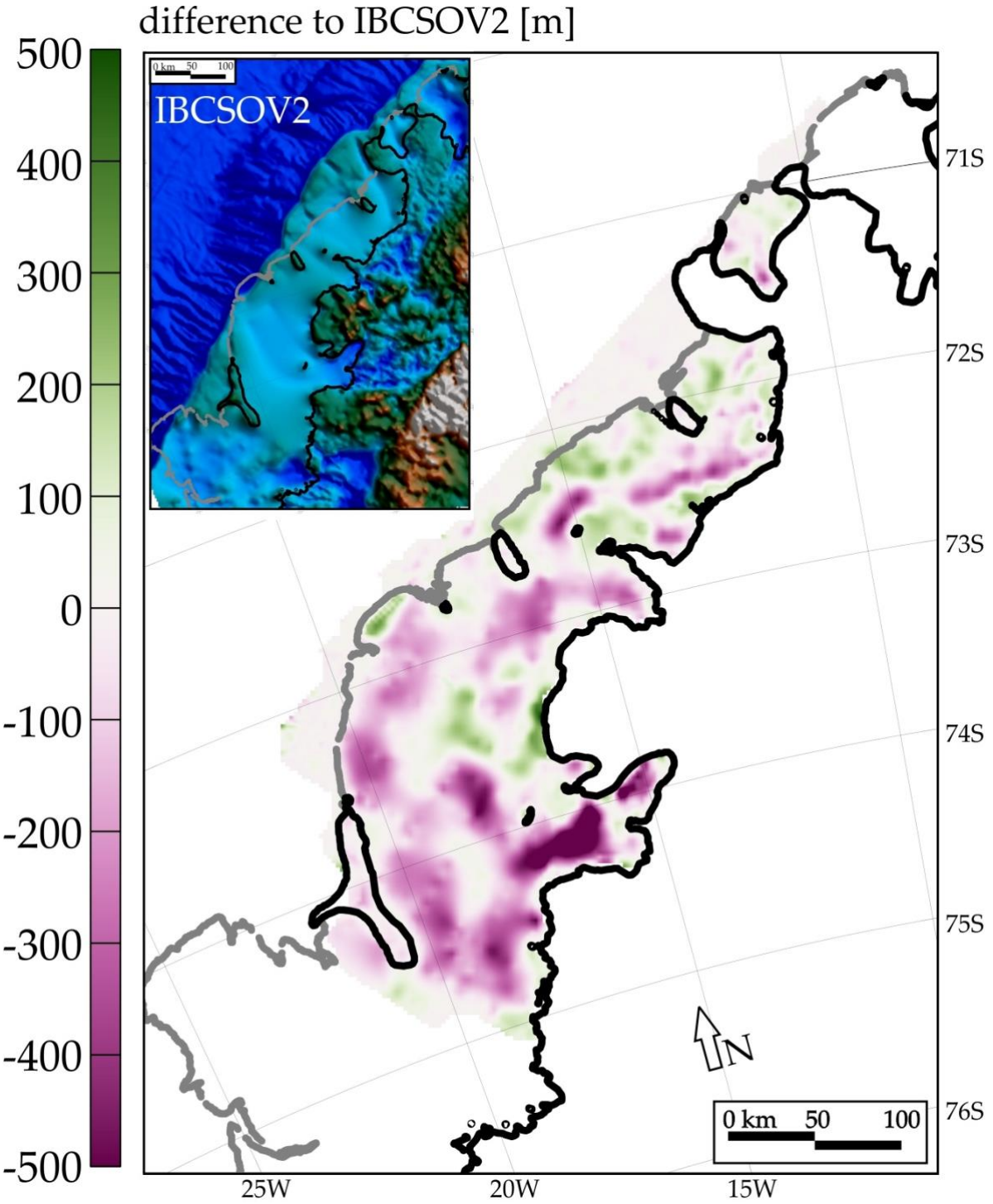

Supplementary Figure 4. Difference of the new modelled bathymetry to topographic compilation IBCSO V2[4]. Topography compilation IBCSOV2 is shown in upper left corner, highlighting smoothly interpolated seabed under the ice shelf using data from open sea and the grounded ice sheet together with steering points[4]. Purple colour code indicates where modelled bathymetry is deeper compared to the topography compilation, while green areas indicate the opposite. Calving fronts and grounded areas in are extracted from MEaSUREs data collection[1] and additional databanks[2].

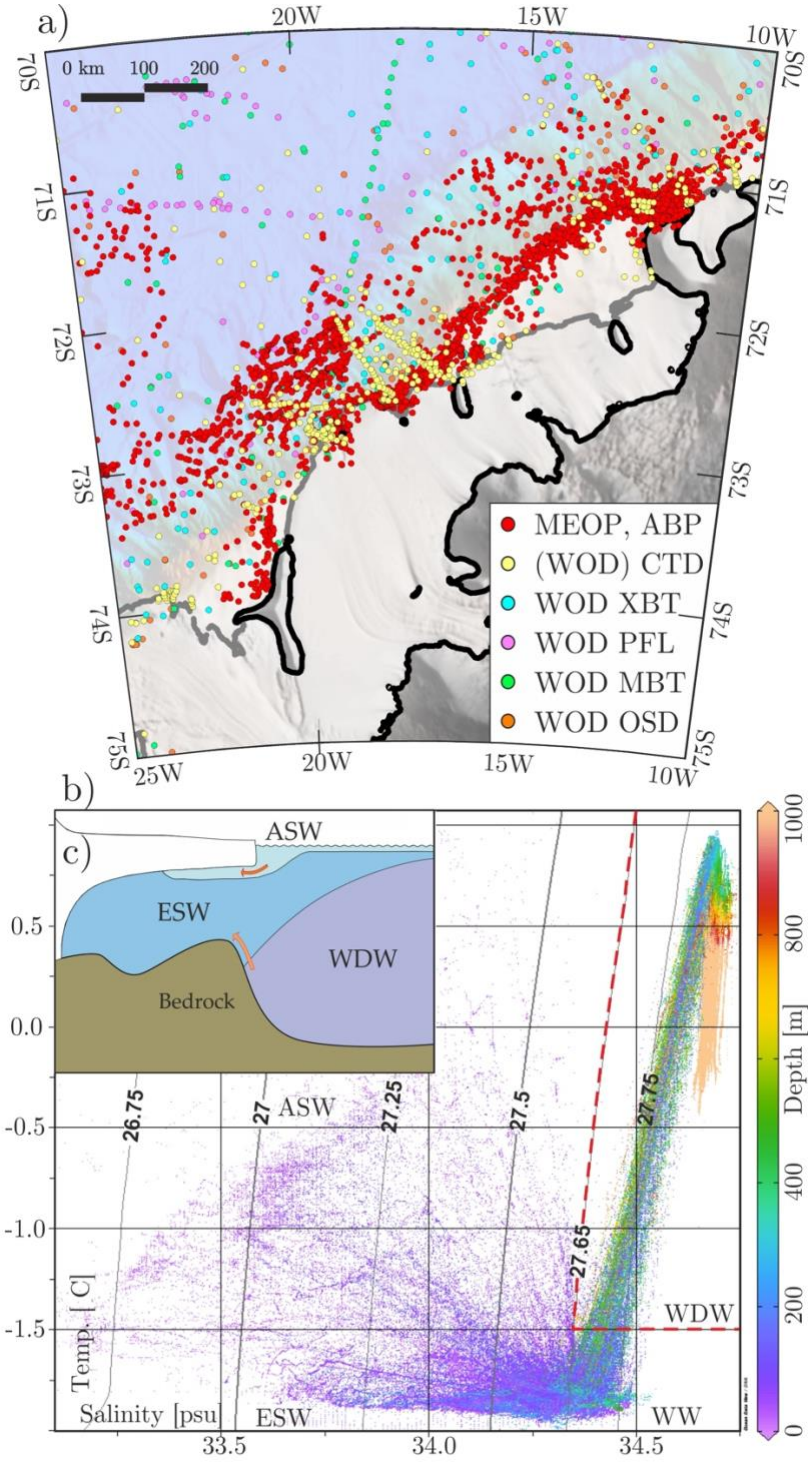

Supplementary Figure 5: Overview of oceanographic data. (a) shows oceanographic data compiled for this study with CTD profiles from World Ocean Database (WOD)[5] and individual additional CTD stations (yellow), marine mammal data MEOP[6] (red), as well as Expendable Bathythermographs (XBT), Profiling Floats (PFL), Mechanical Bathythermographs (MBT), and Ocean Station Data (OSD) from the World Ocean Database[5]. Calving fronts and grounded areas here are extracted from MEaSUREs data collection[1]. (b) shows a T/S diagram using data when both temperature and salinity records were available. Grey contour lines indicate the potential density anomaly in the diagram. Prevalent water masses in the survey area are marked both here and in a simplified sketch in (c), modified[7]. The red dashed line in (b) indicates the classification of WDW (above -1.5°C and above potential density anomaly of 27.65 kg/m^3). ASW, Antarctic Surface Water; ESW, Eastern Shelf Water; WDW, Warm Deep Water; WW, Winter Water.

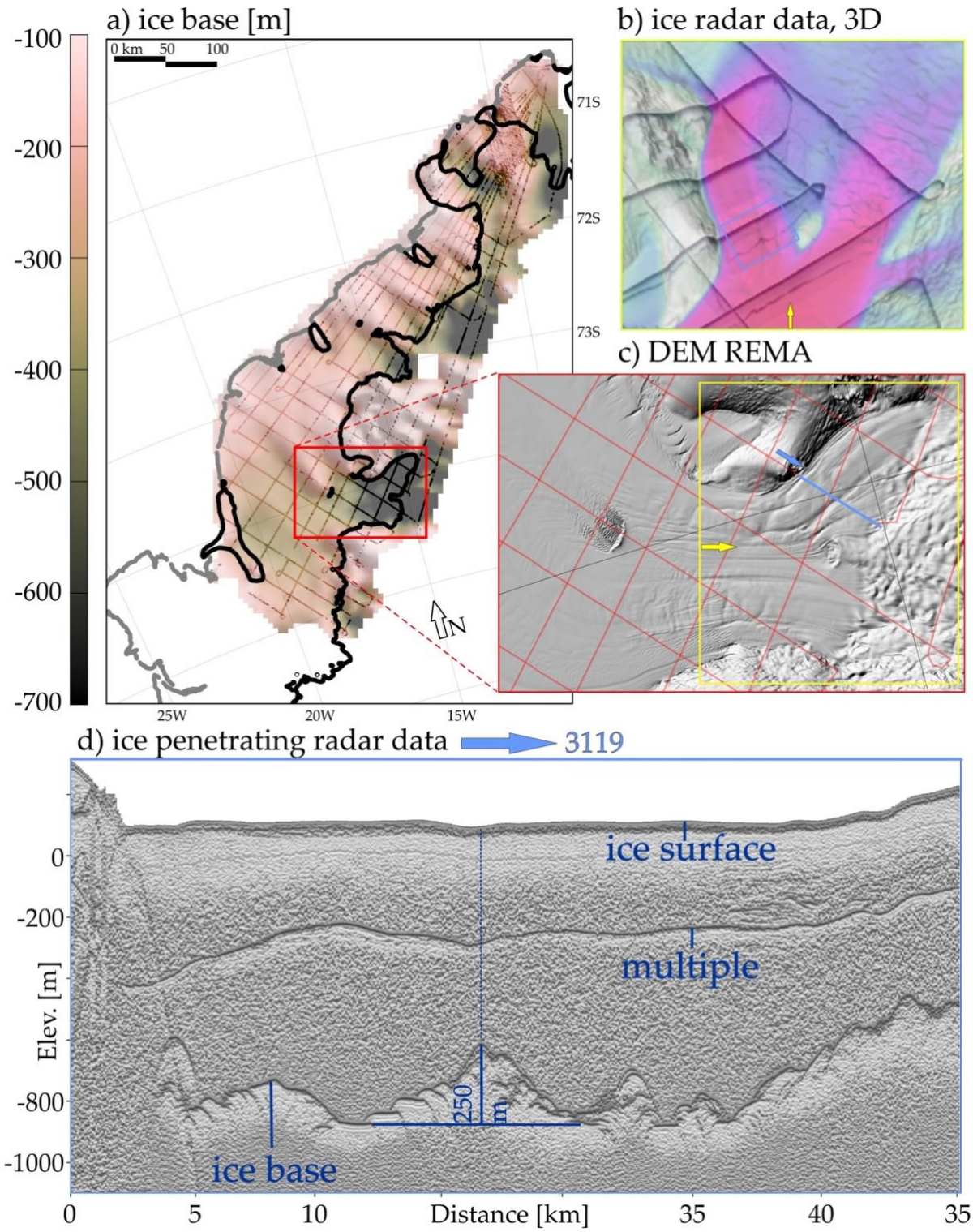

Supplementary Figure 6: Ice base across Riiser-Larsen Ice Shelf from newly acquired ice penetrating radar data with focus on subglacial channels. (a) shows availability of radar data with ice base and marked areas of interest. Calving fronts and grounded areas here are extracted from MEaSUREs data collection[1] and additional databanks[2]. Features within red bounding box at main inlet indicate basal channel formation, see (b) to (d) with: (b) a 3D view on ice penetrating radar data with DEM REMA[3] overlain. Hill shade of REMA[3] is depicted in (c). A radargram in (d) shows basal channel formation coinciding with surface structures with a vertical exaggeration of ~10. The channels reach heights of up to 300 m above their banks, but become smaller downstream, reaching heights of 50 - 100 meters close to the pinning point. Unlike locally grounded ice over a pinning point (Supplementary Fig. 1), ice surface is depressed due to floatation of thinner ice, as indicated by the continued dashed blue line. Its profile location is marked in (b) and (c).

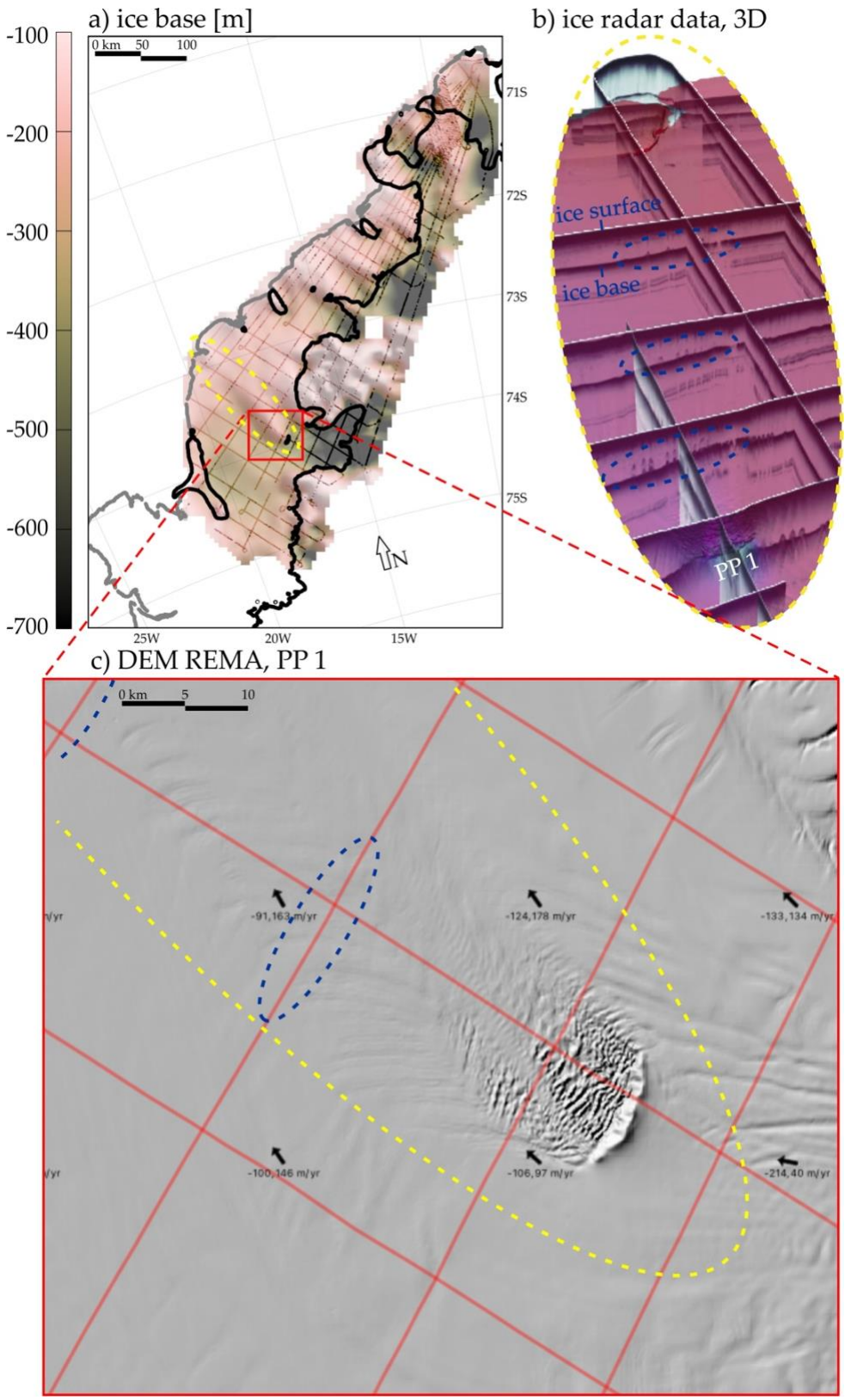

Supplementary Figure 7. Ice base across Riiser-Larsen Ice Shelf from newly acquired ice penetrating radar data with focus on basal melt structures around the central pinning point. (a) shows the ice base position across the survey area. A yellow ellipse here marks the three-dimensional view in (b) of the area in question. It shows the basal melt structures at the ice base on the western side of pinning point 1. (c) depicts hill shade of REMA[3] and ice flow vectors[1] within the red bounding box of (a) and shows the disrupted progression of structures by pinning point 1. While channels phase out to the east, a fan-shaped set of new channels appears to the west of it, with heights of up to 50 m. Calving fronts and grounded areas in (a) are extracted from MEaSUREs data collection[1] and additional databanks[2].

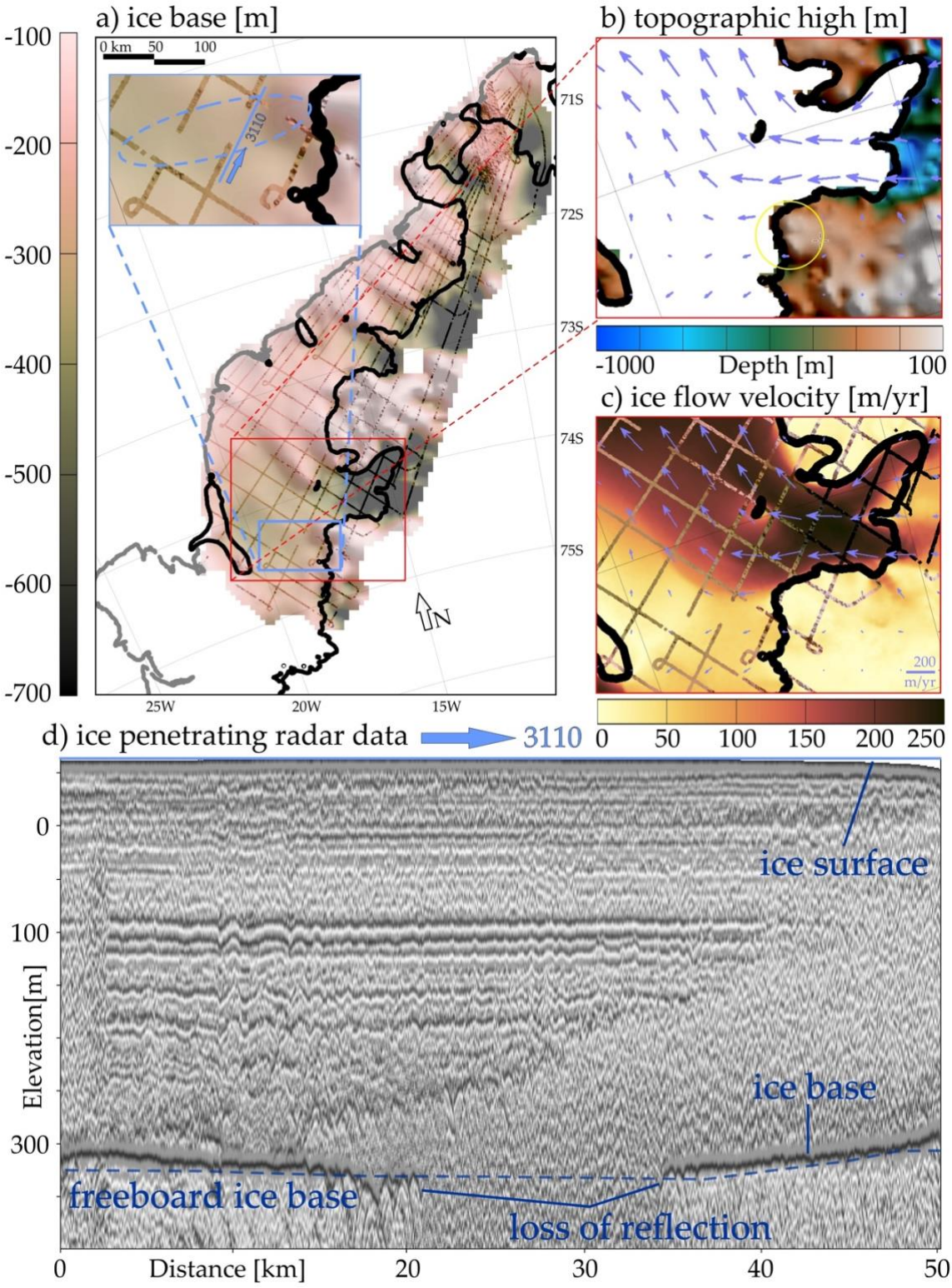

Supplementary Figure 8. Ice base across Riiser-Larsen Ice Shelf from newly acquired ice penetrating radar data with focus on marine ice accretion. (a) shows ice base position across the survey area. A blue bounding box here marks the area of possible marine ice accretion. A loss of reflection at the ice base extends for about 50 km along ice flow with about 5 km width. A topographic high upstream of the area in question is shown in (b) with an elevation of about 300 m above surrounding topographic constraints. The ice flow fields[8] are displayed in (c). Together with accretion rates independently derived from satellite altimetry data[9] (Fig. 1a), we conclude that the absence of ice-base echo represents marine ice here, similar to observations at the Larsen C[10,11] and Ronne ice shelves[12]. (d) shows the radargram of line 3110 along the excerpt of the zoomed-in section of (a). Calving fronts and grounded areas are extracted from MEaSUREs data collection[1] and additional databanks[2].

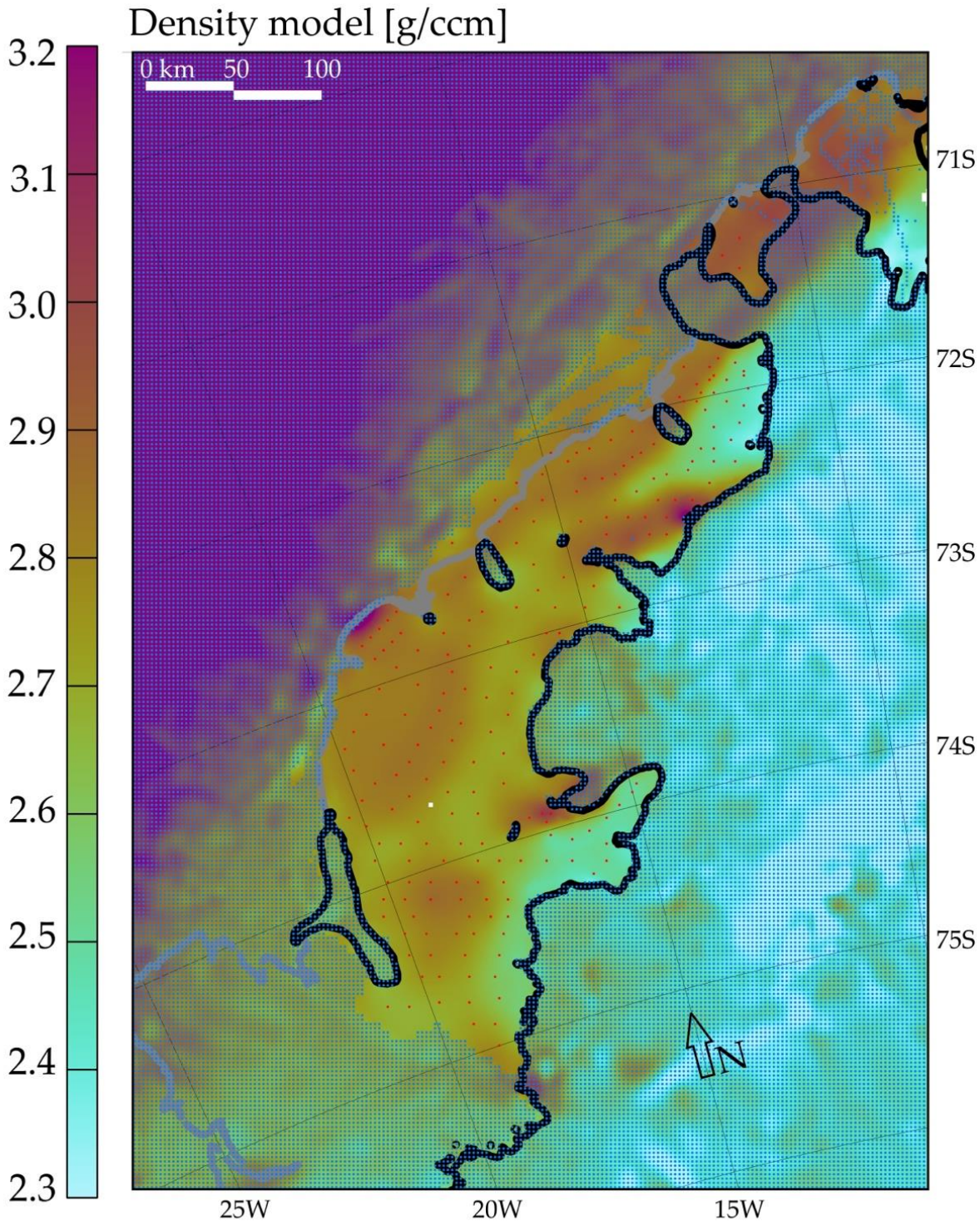

Supplementary Figure 9. Bedrock density model used for inversion. Points of derived density and manually inserted inputs with blue and red points, respectively (see Methods). Calving fronts and grounded areas are extracted from MEaSUREs data collection[1].

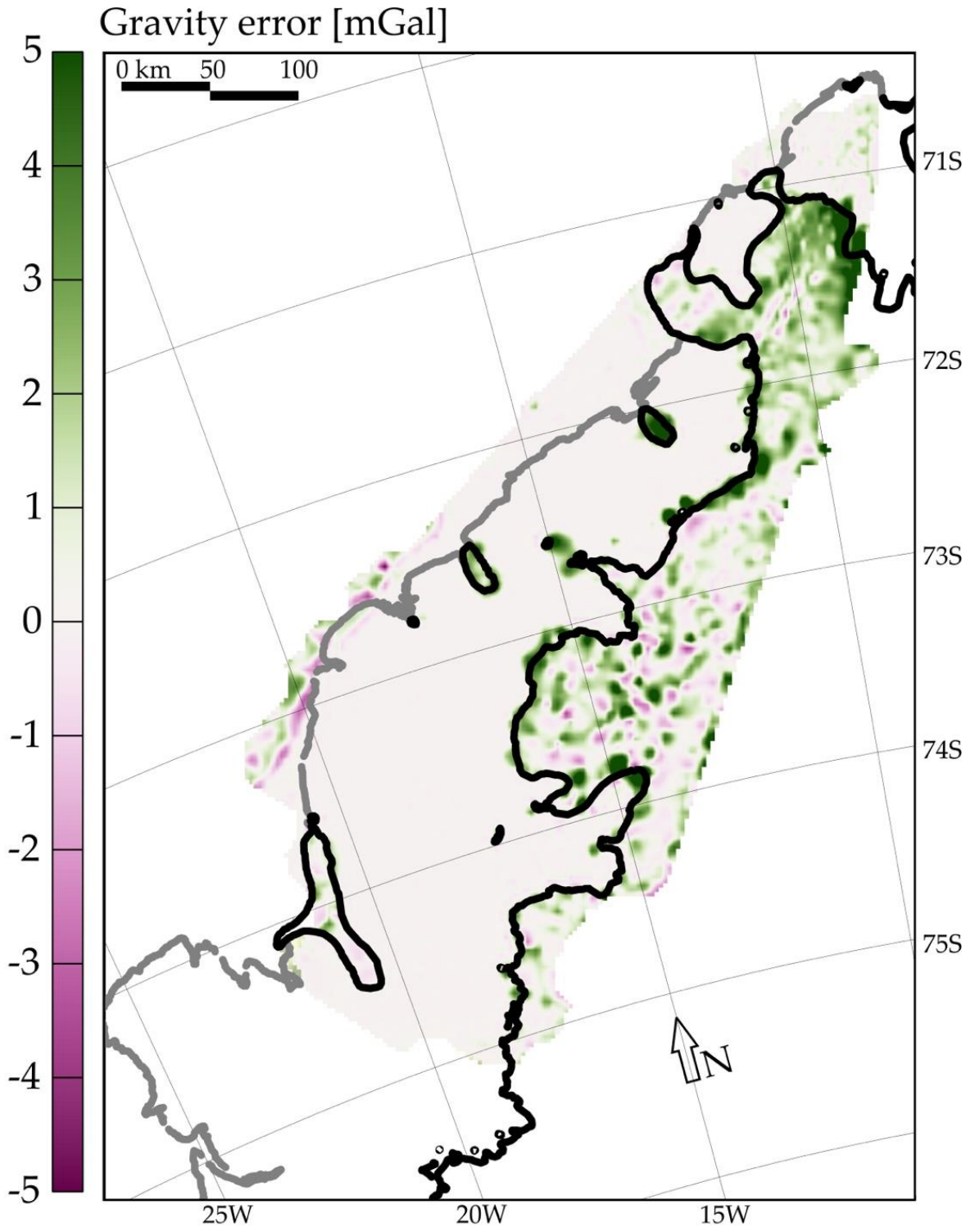

Supplementary Figure 10. Gravity residuals after modelling the Riiser-Larsen Ice Shelf cavity. This visualization is limited to the extent of newly acquired gravity anomaly data. Residuals have a root mean square error of 1.3 mGal with individual peaks of up to 10 mGal gravity inversion. The absence of major residuals implies that the generation of our density model based on a geological interpretation is consistent. Errors are higher in areas of highly-undulating topography, such as grounded regions and at the continental shelf. This is due to (i) differences of spatial resolution in the available bathymetric data and the newly acquired gravity data and (ii) the limiting effect of acquiring gravity data high above the topographic sources. Calving fronts and grounded areas are extracted from MEaSUREs data collection[1].

References

1. Mouginot, J., Rignot, E. & Scheuchl, B. MEaSUREs Antarctic Grounding Line from Differential Satellite Radar Interferometry, Version 2 [Data Set]. Boulder, Colorado USA. NASA National Snow and Ice Data Center Distributed Active Archive Center. https://doi.org/10.5067/IKBWW4RYHF1Q (2016).
2. Moholdt, G. & Matsuoka, K. Inventory of Antarctic ice rises and rumples (version 1) [Dataset]. Norwegian Polar Institute. NPOLAR https://doi.org/10.21334/NPOLAR.2015.9174E644 (2015).
3. Howat, I., Porter, C., Smith, B. E., Noh, M.-J. & Morin, P. The Reference Elevation Model of Antarctica – Mosaics, Version 2. Harvard Dataverse, V1 https://doi.org/10.7910/DVN/EBW8UC (2022).
4. Dorschel, B. *et al.* The International Bathymetric Chart of the Southern Ocean Version 2. *Sci Data* **9**, 275 (2022).
5. Boyer, T. P. *et al.* World Ocean Database 2018.
6. Roquet, F. *et al.* Estimates of the Southern Ocean general circulation improved by animal-borne instruments. *Geophys. Res. Lett.* **40**, 6176–6180 (2013).
7. Hattermann, T., Smedsrud, L. H., Nøst, O. A., Lilly, J. M. & Galton-Fenzi, B. K. Eddy-resolving simulations of the Fimbul Ice Shelf cavity circulation: Basal melting and exchange with open ocean. *Ocean Modelling* **82**, 28–44 (2014).
8. Mouginot, J., Rignot, E. & Scheuchl, B. MEaSUREs Phase-Based Antarctica Ice Velocity Map, Version 1 [Data Set]. Boulder, Colorado USA. NASA National Snow and Ice Data Center Distributed Active Archive Center. https://doi.org/10.5067/PZ3NJ5RXRH10 (2019).
9. Davison, B. J. *et al.* Annual mass budget of Antarctic ice shelves from 1997 to 2021. *Science Advances* **9**, eadi0186 (2023).
10. Kulessa, B., Jansen, D., Luckman, A. J., King, E. C. & Sammonds, P. R. Marine ice regulates the future stability of a large Antarctic ice shelf. *Nat Commun* **5**, 3707 (2014).
11. Kulessa, B. *et al.* Seawater softening of suture zones inhibits fracture propagation in Antarctic ice shelves. *Nat Commun* **10**, 5491 (2019).
12. Lambrecht, A., Sandhäger, H., Vaughan, D. G. & Mayer, C. New ice thickness maps of Filchner–Ronne Ice Shelf, Antarctica, with specific focus on grounding lines and marine ice. *Antartic science* **19**, 521–532 (2007).